Organic Electronics 13 (2012) 789–795

Contents lists available at SciVerse ScienceDirect

Organic Electronics

journal homepage: www.elsevier.com/locate/orgel

Organic field-effect transistors as new paradigm for large-area molecular junctions

Stefano Casalini [a,*], Arian Shehu [a], Silvia Destri [b], William Porzio [b], Maria Cecilia Pasini [b], Francesco Vignali [b], Francesco Borgatti [a], Cristiano Albonetti [a], Francesca Leonardi [c,a], Fabio Biscarini [a]

[a] Consiglio Nazionale delle Ricerche – Istituto per lo Studio dei Materiali Nanostrutturati (CNR-ISMN) via P. Gobetti n. 101, 40129 Bologna, Italy
[b] Consiglio Nazionale delle Ricerche – Istituto per lo Studio delle Macromolecole (CNR-ISMAC) via Bassini n. 15, 20133 Milano, Italy
[c] "Alma Mater Studiorum" Università di Bologna, Dipartimento di Chimica "G. Ciamician" via Zamboni n. 33, 40126 Bologna, Italy

ARTICLE INFO

Article history:
Received 30 August 2011
Received in revised form 20 January 2012
Accepted 23 January 2012
Available online 8 February 2012

Keywords:
SAM
OFET
Charge injection
Molecular junction

ABSTRACT

Self-Assembly Monolayers (SAMs) are considered a promising route for solving technological hindrances (such as bias-stress, contact resistance, charge trapping) affecting the electrical performances of the Organic Field-Effect Transistors (OFETs). Here we use an OFET based on pentacene thin film to investigate the charge transport across conjugated SAMs at the Au/pentacene interface. We synthesized a homolog series of π-conjugated molecules, termed Tn-C8-SH, consisting of a *n*-unit oligothienyl Tn ($n = 1..4$) bound to an octane-1-thiol (C8-SH) chain that self-assembles on the Au electrodes. The multi-parametric response of such devices yields an exponential behavior of the field-effect mobility (μ), current density (J), and total resistivity (R), due to the SAM at the charge injection interface (i.e. Au-SAM-pentacene). The surface treatment of the OFETs induces a clear stabilization of different parameters, like sub-threshold slope and threshold voltage, thanks to standardized steps in the fabrication process.

1. Introduction

Among a variety of molecular junction configurations explored for probing directly molecular charge tunneling [1,2], the vertical molecular junction based on Au/SAM/Au has proven reproducible, robust, scalable to large area, and aligned to planar technology standards [3]. Before the deposition of the top metal contact, this configuration requires a conductive buffer layer (typically PEDOT:PSS) against short circuits that usually affect the fabrication of nano-junctions. However, this buffer layer limits the choice of SAMs on conductive polymer.

On the other hand, the use of SAMs in the interface engineering has been largely exploited for tuning the electrical performances of OFETs, especially to modify the chemical–physical properties of interfaces such as electrode-organic semiconductor (OS) and/or dielectric-OS [4]. In particular, it was recently demonstrated that OFETs with alkanethiol SAM-functionalized source–drain electrodes respond as molecular gauge in saturation regime [5]. The detailed features of the trend of the charge mobility vs the number, *n*, of methylene units arise from an interplay of interfacial morphology [6], molecular ordering, decrease of energy disorder, and charge tunneling mediated by the SAM alkyl chain. The latter yields odd–even fluctuations of the charge mobility vs *n* [5]. It follows that OFETs with systematic Au electrode functionalization (Au-SAM-OS-SAM-Au) can be used to rationalize the charge injection into SAMs alternatively to the standard molecular junctions with SAM sandwiched between two metal electrodes. The former has clearly a more complex architecture than the latter, but the FET configuration allows the same reliability of large-molecular junctions (close to 100%) without any hindrance for scaling up the total area (in

* Corresponding author.
E-mail address: s.casalini@bo.ismn.cnr.it (S. Casalini).

1566-1199/$ - see front matter © 2012 Elsevier B.V. All rights reserved.
doi:10.1016/j.orgel.2012.01.020

our case around 100 μm^2). Moreover the FET configuration offers, generally speaking, a precise tuning of the charge density at the contact interfaces compared to the traditional junctions. This is feasible because it has two variable biases (i.e. gate–source – V_{GS} – and drain–source – V_{DS} – voltages) and the charge carriers (holes or electrons) can be selected by choosing the OS.

In this work, we have investigated how the charge injection is affected by the presence of the oligothiophene-based SAMs in a real device (i.e. pentacene FET) and we proved experimentally that the exponential decay β measured from OFET is in agreement to the one obtained in the ideal molecular junctions (metal–insulator–metal).

2. Experimental

For these purposes, we designed a π-conjugated alkanethiol, Tn-C8-SH, with an increasing number of thienyl units from $n = 1$ to $n = 4$ bound to an octane-1-thiol tail (see Appendix A) [7–9]. The chemical structure of the homolog series consists of: (i) a thiol as "tail group" binding the polycrystalline gold film [10,11], (ii) an alkyl chain with eight methylene units, to provide sufficient packing energy and guarantee optimal charge injection in pentacene/SAM FETs [5], (iii) the *n*-thienyl ($n = 1 \ldots 4$) conjugated "head-group" to introduce attractive π–π and repulsive steric interactions as well as to vary systematically the SAM length (see Fig. A1) This multifunctional SAM integrates the self-assembly tendency of the octane-1-thiol and the more efficient charge transfer of the π-conjugated system [12].

The schematics of the bottom-electrode device layout is shown in Fig. B1. Pentacene ultra thin films 15 nm thick (equivalent to 10 monolayers – ML – of pentacene) are grown by high vacuum sublimation on test-patterns with Au electrodes functionalized with Tn-C8-SH (see Appendix B). The film morphology is characterized by Atomic Force Microscopy (AFM) through the dynamic scaling parameters: saturated root mean square (rms) roughness (σ_{rms}), correlation length (ξ) and roughness exponent (α) (see Appendix B, Fig. B2) [13–15]. They exhibit the Frank Van der Merwe growth mode on the transistor channel [16] whereas a crystalline growth onto the polycrystalline SAM-coated Au [17].

3. Results and discussion

FET transfer and output characteristics (see Fig. 1) were acquired *ex situ* in a high-vacuum chamber featuring three motorized electrical contact probes. Vacuum conditions are reported in the Appendix B. The electrical characteristics have been averaged on 64 and 40 test devices for C8-functionalized and bare-Au respectively, whereas each oligothiophene functionalization has been averaged on 10–20 devices.

From the transfer and output characteristics, we can fully describe the electrical performances of OFETs. The bare and C8-SH functionalized OFETs show an ohmic behavior mainly highlighted by the I_{DS} linear-dependence of the output characteristics in the linear regime [18]. In particular C8-SH stabilizes the transfer characteristics as shown by the clear decrease of the I_{DS} errors in the *I–V* graphs (see Fig. 1A). The addition of thiophene rings, Tn-C8-SH ($n = 1 \ldots 4$), affects clearly the electrical features. The output characteristics show a progressive worsening of the ohmic contacts in the linear regime together with the weakening of the I_{DS} values (from mA to μA). This effect is maximized for devices with T4-C8-SH-coated electrodes where hysteresis appears in the output characteristics (Fig. 1B). Conversely the transfer characteristics (see Fig. 1A) show a marked decrease of the off-current, the shift of the turn-on voltage closer to zero and the decrease of the sub-threshold slope of 3–5 times with respect to the reference FET devices increasing the SAM thickness.

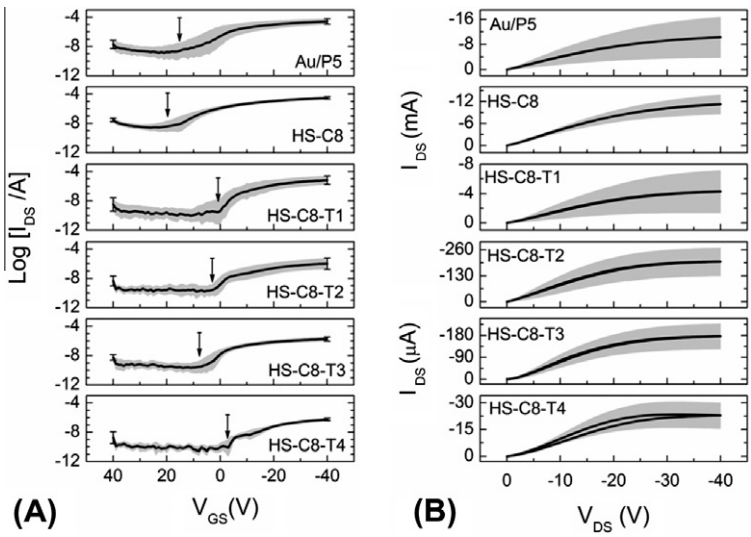

Fig. 1. Transfer and output characteristics dataset. (A) The continuous line is the logarithmic mean, gray shaded area is the envelope of the rms fluctuations. The pointer indicates the turn-on voltage. (B) The continuous line is the mean trend and the gray shaded area is the rms fluctuations.

These experimental evidences indicate an overall stabilization of the electrical behavior due to a reduction of the trap density [19].

Fig. 2A shows the charge carrier mobility, μ (holes for pentacene) as extracted from the transfer characteristics in linear and saturation regime. It exhibits an exponential decay from C8-SH ($n = 0$) to T4-C8-SH ($n = 4$). Within the experimental errors, we cannot resolve the presence of odd–even effects in the charge mobility [20]. We extract the inverse exponential decay length scale β as the slope of the linear fitting of the log-lin plot of the charge mobility vs number n of thienyl units. The molecular length has been calculated by the sum of the C8-SH (14 Å) plus 4 Å for each thienyl units calculated by dividing the length of sexithienyl by six [21,22]. The correctness of such estimate is confirmed by a sum of bond lengths (see Fig. 2). The inverse length scale β turns out to be $0.24(\pm 0.01)\,\text{Å}^{-1}$ in the linear regime and $0.17(\pm 0.02)\,\text{Å}^{-1}$ in saturation regime. These values are consistent with two-point-contact current measurements on π-systems [1,2,12,23] because the conjugated molecules have higher conductivity than the aliphatic thiols at the molecular scale due to a lower HOMO–LUMO gap (around 3 eV). For this reason the decay exponent β of π-conjugated molecules ranges from 0.2 to $0.6\,\text{Å}^{-1}$, while for the saturated molecules ranges from 0.6 to $1.1\,\text{Å}^{-1}$ [2]. OFETs show high sensitivity with respect to the charge injection at the interface; we have evaluated a β around $0.2\,\text{Å}^{-1}$ in both regimes for the oligothiophene SAMs and β around $0.6\,\text{Å}^{-1}$ for the homolog series of alkanethiols in saturation regime [5]. The exponential decay of the charge carrier mobility agrees with the data in literature [2,24] and it suggests a through-bond charge tunneling through the SAM moiety. Further investigations must be undertaken in order to characterize more precisely which kind of mechanism occurs during the charge injection, as shown by Wang et al. [24] No marked odd–even effect is observed indicating that straight oligothienyl linear chains dominate, sigma bond isomerization is negligible within the molecules in the SAM, and there are no substantial differences in tilt angle along the homolog series. As comparison, we have extracted from the output characteristics the current density J, by dividing the OFET current (in both regimes) by the width W multiplied by the thickness h of the charge transport layer (see Fig. 2B). From morphological measurements, the area of the active layer is formed by the width of the transistor channel multiplied by the pentacene monolayers involved in the electrical transport. As proved recently, three MLs are active in pentacene-based devices, therefore the thickness of the active area is 4.5 nm [14]. The estimated area in our devices is 100 and 50 μm^2 for the two different test-pattern geometries (channel length – L and width – W are 20 μm/11200 μm and 40 μm/22400 μm, respectively). The current density is estimated at $V_{GS} = -40$ V, for $V_{DS} = -1$ V and $V_{DS} = -40$ V corresponding to the linear and saturation regimes respectively. The exponential decay β measured from the current density for both regimes matches the values extracted from the charge mobility (0.27 and $0.23\,\text{Å}^{-1}$ for linear and saturation regime respectively).

The FET current (I_{DS}) depends on three in-series resistors with two representing the source and drain interfaces with the organic semiconductor (R_{SD}), and the other one is the resistance of the channel (R_{ch}), $R = R_{ch} + R_{SD}$. There are different ways for the extraction of the contact resistance, viz. transfer line method (TLM) [25], gated four-probe measurements [26] and local potentiometry [27]. We have evaluated the effective resistivity of our devices through the relationship $R \times W = (V_{DS}/I_{DS}) \times W$ where W is the channel width. Moreover, in the linear regime, the contributions of the charge injection interfaces to the effective resistance will be the larger, as lowering of the injection barrier due to negligible effect of the longitudinal electric field. As shown in Fig. 3A, the trend of the effective resistivity is clearly exponential. In order to extract the parameter, we fit the resistivity according two schemes:

(i) with an exponential function $R \times W = R_0 \exp(\beta n)$, where R_0 is the resistivity related to $n = 0$. Best fit yields $R_0 * W = 0.6(\pm 0.2)\,\text{k}\Omega\,\text{m}$ and $\beta = 0.25 \pm 0.04\,\text{Å}^{-1}$ matching the value extracted from both the mobility μ and the current density J vs number of thienyl units. This kind of fit cannot allow us to identify the two distinct contributions of source and drain electrodes.

(ii) with the phenomenological fit function $R \times W = R_{ch} + R_0 \exp(\beta n)$.

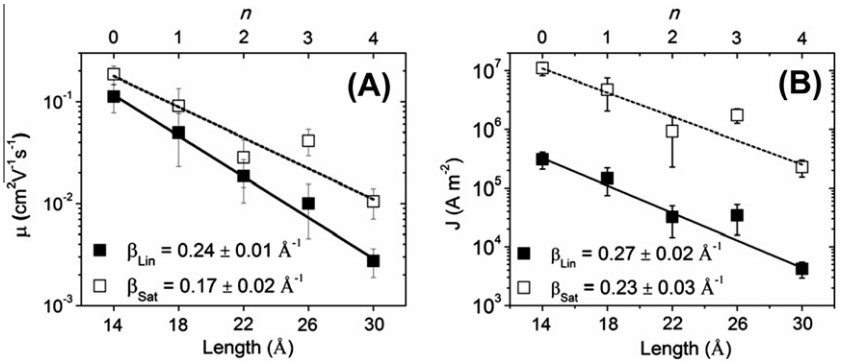

Fig. 2. Exponential decay vs. SAM thickness (bottom axis) and number n of thienyl units in the SAM (top axis). (A) The field-effect mobility values are extracted from the transfer characteristics in the linear (full squares) and saturation (empty squares) regimes. (B) The charge density are extracted from the output characteristics in the linear (full squares) and saturation (empty squares) regimes.

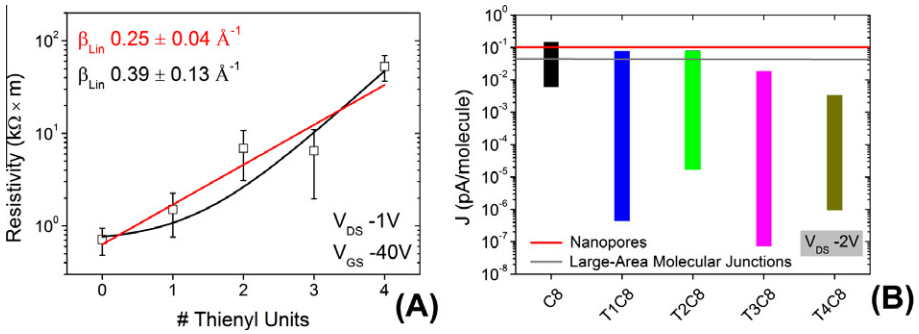

Fig. 3. Plot of the resistivity and charge density per molecule vs. SAM length. (A) Continuous red line is exponential fit, continuous black line is exponential with an offset. The values are extracted from the output characteristics in linear regime. (B) The current density of nanopores (red line) and large area molecular junctions (gray line) are shown as reference [1]. The bars for the different SAMs span the range corresponding to the gate voltage between 0 V and −40 V (discrete data points acquired with pitch −5 V). (For interpretation of the references to color in this figure legend, the reader is referred to the web version of this article.)

Here R_{ch} can be estimated as $R_{ch} = \frac{L}{[W \cdot \mu_{lin} \cdot C_d \cdot (V_{GS} - V_{th})]}$, where the pentacene charge mobility μ_{lin} should be taken in the absence of the electrodes as independent on n. For $\mu_{lin} = 0.1–1\ cm^2/(V\ s)$, $R_{ch} * W \approx 0.05–0.5\ k\Omega\ m$. The best fit of the data in Fig. 3A yields: $R_{ch} * W = 0.7(\pm 0.3)\ k\Omega\ m$, $R_0 * W = 0.08(\pm 0.2)\ k\Omega\ m$, $\beta = 0.4(\pm 0.1)\ Å^{-1}$. Such β value is in agreement with the other measurements and it is a direct evidence of the control exerted by the charge injection interfaces on the overall current.

Lastly, Fig. 3B shows the current density per molecule for different functionalization. Current density is estimated as the ratio between the drain-source current and the number of molecules active in the charge injection. We assume the number of molecules per unit area as reported in literature: $7.6 \times 10^{-10}\ mol/cm^2$ for C8-SH [11,28] and $6.0 \times 10^{-10}\ mol/cm^2$ for the Tn-C8-SH [29]. In the latter the density does not depends on n. For each SAM the current density across a single molecule undergoes a modulation vs. gate voltage by several orders of magnitude, and it is possible to span ultra-low currents across a single molecule. With respect to experimental data acquired from nanopores and large-area molecular junctions biased to 0.2 V, OFETs show comparable current per molecule at highest gate voltage (−40 V). This suggests that these SAMs experience an effective potential drop across the charge injection interface around 0.2 V [3].

4. Conclusions

In conclusion, OFETs are extremely sensitive to charge injection on the molecular scale at the metal/semiconductor interface. Our experiment shows that SAM-assisted charge tunneling is the relevant mechanism for enhancing the charge injection across the metal/SAM/OS interface. These results show that the SAM-functionalized electrodes in the OFET behave as a molecular junction, introducing OFET as tool for studying the charge injection through self-assembly monolayers. In addition the inverse decay length in π-conjugated has been verified by three parameters such as mobility, charge density and resistivity. Although these results were already obtained in different ways such as Conductive Probe Microscopies, nano-junctions, molecular junctions etc., the OFETs are a reproducible setup suitable for standardization and upscaling.

Beyond the information on charge transport mechanism at the molecular scale, the conjugated SAMs in OFETs yield a marked improvement of several technologically relevant OFET parameters in terms of absolute and spread values. This clearly indicates that SAMs in OFETs provide a viable route for standardizing OFET performances.

Acknowledgement

We would like to dedicate this work to Prof. Carlo Taliani in occasion of his retirement. We thank D. de Leeuw and H. Akkermann for providing us original data on molecular junctions. This work is supported by EC FP7 ONE-P Large Scale project no. 212311.

Appendix A

A.1. Tn-C8-SH Synthesis

Octanethiol has been purchased from Sigma–Aldrich. The oligo-thiophenes thiols are synthesized as described in the following.

A series of α oligothiophene derivatives Tn-C8-SH (n ranging from 1 to 4), where the chain links an oligothienyl to a thiol functionality, was synthesized. Thiophene and 2,2′-bithiophene were lithiated to 2-lithiothiophene and 5-lithio-2,2′-bithiophene, respectively, and alkylated with a 3 to 5-fold excess of 1,8-dibromooctane [30]. The alkylation gave 52–58% of the desired alkyl-substituted oligothiophene with a terminal bromide group Fig. A1.

To obtain the superior oligothienyl homologs (n = 3 and 4) the alkylated bithiophene derivative was brominated in the free α-position using N-bromosuccinimide (NBS) in chloroform [31] at room temperature and gave the regioselectively brominated thiophene derivative 5-Bromo-5′-(8 -bromooctyl)-2,2′-bithiophene (1) (84–92% yield).

The α-T3 derivative was obtained via standard Stille coupling between (1) and 2-(tributylstannyl) thiophene (Aldrich) (60% yield) while the α-T4 derivative was

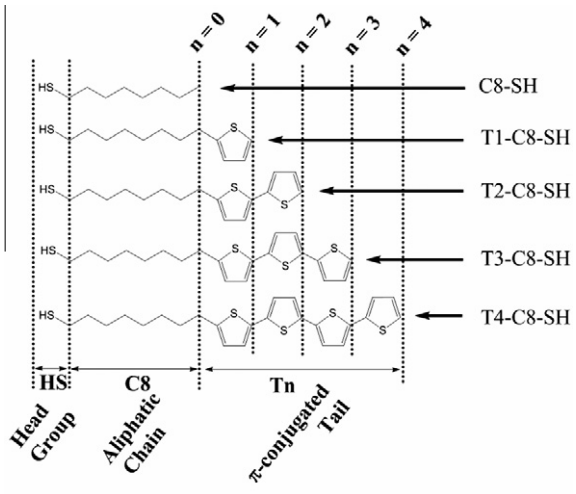

Fig. A1. The homolog serie of the oligothienyl thiols, Tn-C8-SH.

obtained via Suzuky coupling between 2,2′-Bithiophene-5-boronic acid pinacol ester (Aldrich) and (1) (40% yield).

Conversion to the thiol was performed via formation of a thioacetic acid ester derivative (2) obtained by refluxing a mixture of potassium thioacetate (10-fold excess) and the corresponding Br-alkyl-oligothienyl in THF, followed by reduction of (2) with LiAlH4 (Yield varying from 60% to 30% starting from the shortest oligomer $n = 1$ to the longest one $n = 4$) (30).

A.2. General procedure for thiol formation

LiAlH4 (1 M in THF, 2 eq) was added dropwise to a stirred solution of thioacetic acid ester derivative (1 eq) in THF, keeping the temperature at 0 °C. The reaction mixture was stirred for 30 min at RT, a few drops of AcOEt were added, and stirring was continued for further 30 min. 3 M HCl was added, and the resulting mixture was extracted with $CHCl_3$. The organic phase was washed with water, dried (Na_2SO_4), and then evaporated to dry. Flash chromatography of the residue (silica gel, hexane/CH_2Cl_2) gave the title compound.

8-(thien-2-yl)-oct-1-ylthiol (TC8SH): 1H NMR (CDCl3, TMS/ ppm) δ 7.16 (dd, $J = 5.2$ Hz, $J = 1.2$ Hz, 1H), 7.10 (dd, $J = 5.2$ Hz, $J = 3.6$ Hz, 1H), 6.67 (br, 1H), 2.75 (*t*, $J = 7.5$ Hz, 2H), 2.46 (*m*, 2H), 1.69–1.50 (*m*, 4H), 1.36–1.29 (br; 8H). MS, m/e 228 (M+). Oil Yield 50%.

8-(2,2′-bithien-5-yl)-oct-1-ylthiol(T2C8SH): 1H NMR (CDCl3, TMS/ ppm) δ 7.16 (dd, $J = 5.1$ Hz, $J = 1.16$ Hz, 1H), 7.10 (dd, $J = 3.6$ Hz, $J = 1.15$ Hz, 1H), 7.00–6.97 (br, 2H), 6.67 (dt, $J = 3.6$ Hz, $J = 0.8$ Hz, 1H), 2.75 (*t*, $J = 7.5$ Hz, 2H), 2.46 (*m*, 2H), 1.69–1.50 (*m*, 4H), 1.36–1.29 (br; 8H). MS, m/e 310 (M+). Deliquescent Yield 55%.

8-(2,2′:5′,2″-terterthien-5-yl)-oct-1-ylthiol(T3C8SH):;1H NMR (CD2Cl2, TMS/ ppm) δ 7.20 (dd, $J = 5.1$ Hz, $J = 1.16$ Hz, 1H), 7.14 (dd, $J = 3.6$ Hz, $J = 1.16$ Hz, 1H), 7.03 (d, $J = 3.6$ Hz, 1H), 7.00–6.95 (*m*, 3H),6.66 (dt, $J = 3.6$ Hz, $J = 0.8$ Hz, 1H), 2.75 (*t*, $J = 7.5$ Hz, 2H), 2.46 (*m*, 2H), 1.69–1.50 (*m*, 4H), 1.36–1.29 (br; 8H). MS, m/e 392.1 (M+), mp 79.5–81.7 °C. Yield 60%.

8-(2,2′:5′,2″:5″,2‴-quaterthien-5-yl)-oct-1-ylthiol (T4C 8SH), 1H NMR (CDCl3, TMS/ ppm) δ 7.21 (dd, $J = 5.2$ Hz, $J = 1.2$ Hz, 1H), 7.16 (dd, $J = 3.6$ Hz, $J = 1.2$ Hz, 1H), 7.13–6.97 (*m*, 6H), 6.81 (dt, $J = 3.6$ Hz, $J = 0.8$ Hz, 1H),2.79 (*t*, $J = 7.5$ Hz, 2H), 2.53 (*m*, 2H), 1.69–1.50 (*m*, 4H), 1.36–1.29 (br; 8H). MS, m/e 474.1 (M+); mp 141–144 °C. Yield 30%.

Gas-Chromatography coupled by Mass-Spectroscopy has been used to check the products of the synthesis. The level of purity of T1-C8-SH, T2-C8-SH and T3-C8-SH is 99%, whereas T4-C8-SH contains two products of the T2-C8-SH alkylation. These two unknown impurities are not thiolated, therefore they are not able to self-assemble through a covalent bond with Au surface. The abundant rinsing of our test-patterns after the functionalization protocol guarantees from any presence of contaminants in the SAM.

Appendix B

B.1. Functionalization and fabrication of OFETs

Test-Pattern (TP) are fabricated on Si < 100 > n-type (doped by Sb), 500 μm thick, with a resistivity of 0.01–0.03 $\Omega \times$ cm. The dielectric layer is 200 nm thick thermal SiOx. The Au electrodes (125 ± 25 nm) thick are deposited on an adhesive layer of Cr (3–5 nm) on SiOx Fig. B1.

The TP is cleaned following this protocol: (i) photoresist is washed with 10 ml of acetone, (ii) 15 min of piranha solution (H_2SO_4conc:H_2O_2, ratio (1:1) at 65 °C, (iii) dip the TP for 5 s in HF 4% v/v. Every step is followed by nitrogen flow in order to guarantee a dried surface. TPs are stored in CH_2Cl_2 solution prior incubation.

TPs are incubated in ethanol solutions for 72 h. Concentrations range from 1 mM for octanethiol to 0.1 mM for Tn-C8-SH. TPs are rinsed with ethanol and dichloromethane in sequence, to wash away physisorbed molecular aggregates.

Pentacene thin films are deposited on TPs by vacuum sublimation, at a base pressure of 7×10^{-8} mbar. The deposition occurs at a constant rate of 37 Å min^{-1} (2.5 ML min^{-1}) and is stopped at a final pentacene layer thickness equal to 15 nm = 10 ML with the substrate kept at RT. OFET characterization in air and vacuum (10^{-4} mbar) was carried out in a home-built probe station in high vacuum.

B.2. Wettability of polycrystalline Au functionalized by Tn-C8-SH

Using different solvents such as bi-distilled water, ethylene glycol and nitromethane, it has been extracted the adhesion work, W_A, which has been plotted vs. the number of thienyl units (as you can see in Fig. B2).

An abrupt decrease of W_A occurs for the addition of the first thienyl group (from $n = 0$, C8-SH, to $n = 1$, T1-C8-SH). Looking at the overall plot, it is shown a non-monotonic behavior featuring a minimum centered at $n = 2$ (T2-C8-SH) and a maximum at $n = 0$ (C8-SH). This contact angle study has directly assessed the quality of our surface

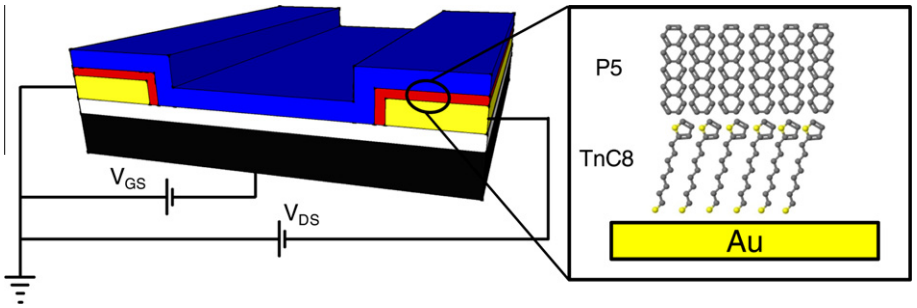

Fig. B1. Schematic view of the pentacene/SAM FET. On the left, the bottom-gate/bottom-contact configuration of the test pattern is shown: black is Si(n+), white SiOx, yellow Au electrodes, red SAMs, blue pentacene (pentacene) layer. Right: a magnification of the Au/T1-C8-SH/pentacene interface. (For interpretation of the references to color in this figure legend, the reader is referred to the web version of this article.)

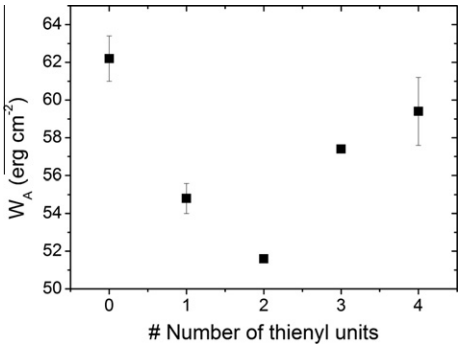

Fig. B2. Work of adhesion is plotted versus the number of thienyl units.

treatments as well as their discrepancies in terms of adhesion work.

B.3. Pentacene thin film morphology on TPs

The morphology of the pentacene thin-film has been verified on SAM-functionalized electrodes and on gate dielectric (see Fig. B3).

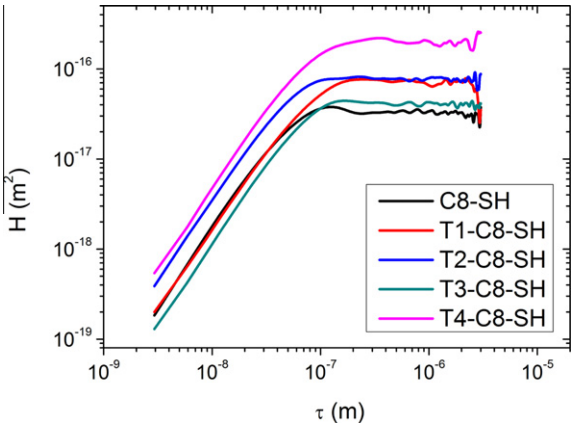

Fig. B4. Overlay of the HHCFs for the different functionalizations of the electrodes.

These images have been analyzed by means of height-height correlation function, H(τ), in which τ is the distance between two points of the image. We have extracted three parameters: (i) the saturated roughness (σ_{rms}) relative to

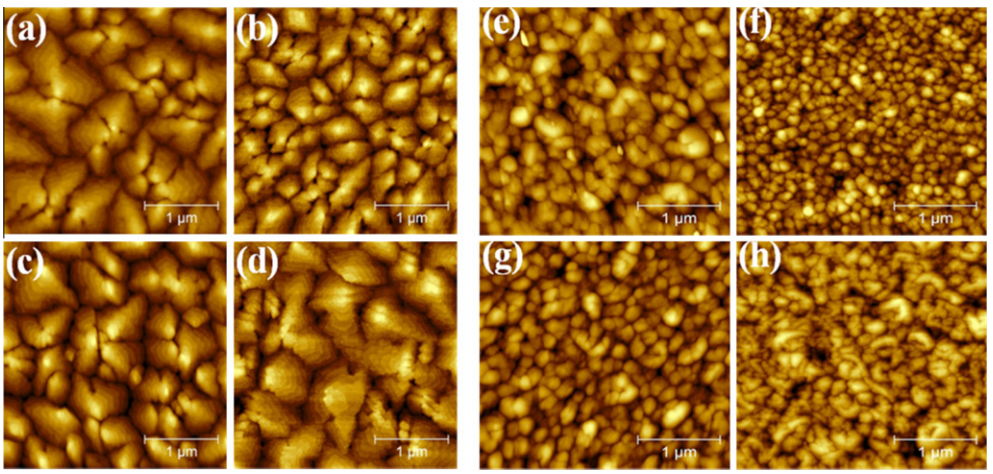

Fig. B3. Morphology of pentacene 10 ML thick film. (a–d), Pentacene on channel. (e–h), Pentacene on polycrystalline Au film. (a and e), T1-C8-SH; (b and f), T2-C8-SH; (c and g), T3-C8-SH and d,h, T4-C8-SH functionalization respectively.

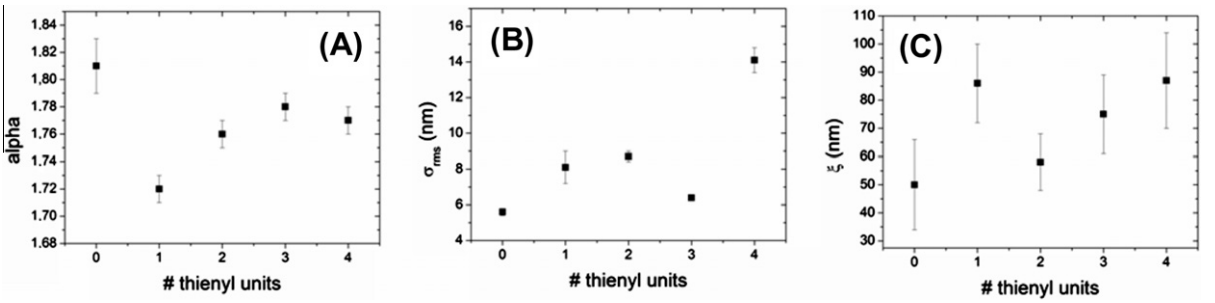

Fig. B5. Alpha coefficient (A), saturated roughness (B) and correlation length (C) have been plotted versus the number of thienyl units.

the plateau of the function, (ii) the roughness coefficient (α), which is the slope of the τ-dependent decaying branch and (iii) the correlation length (ξ) that is the intersection between the plateau and τ-dependent decaying branch projections (Fig. B4).

The first two parameters turn out to be dependent on the different SAMs, on contrary ξ does not resolve the different SAM due to high deviation standards (see Fig. B5).

The pentacene morphology in the channel is invariant for all the devices, because the oligothiophene molecules are not able to link the silicon oxide. As a result of the high level of morphological order of pentacene film, we can extract two correlation lengths: (1) the first one is relative to the size of the islands (105 ± 13 nm) and (2) the second one is representative of the terraces extension (equal to 6 ± 5 nm). Through this AFM image processing, we have assessed the macroscopic difference of the pentacene growth on channel and electrodes as well as the microscopic discrepancies induced by the SAM-coated electrodes.

References

[1] H.B. Akkerman, B. de Boer, Journal of Physics: Condensed Matter 20 (2008) 1–20.
[2] A. Salomon, D. Cahen, S. Lindsay, J. Tomfohr, V.B. Engelkes, C.D. Frisbie, Advanced Materials 15 (2003) 1881–1890.
[3] H.B. Akkerman, P.W.M. Blom, D.M.D. Leeuw, B.D. Boer, Nature 441 (2006) 69–72.
[4] C. -an Di, Y. Liu, G.U.I. Yu, D. Zhu, Accounts of Chemical Research 42 (2009) 1573–1583.
[5] P. Stoliar, R. Kshirsagar, M. Massi, P. Annibale, C. Albonetti, D.M.D. Leeuw, F. Biscarini, Journal of the American Chemical Society 129 (2007) 6477–6484.
[6] C. Albonetti, S. Casalini, F. Borgatti, L. Floreano, F. Biscarini, Chem. Commun. (Cambridge, England) 47 (2011) 8823–8825
[7] C. Nogues, P. Lang, M.R. Vilar, B. Desbat, T. Buffeteau, Colloids and Surfaces A: Physicochemical and Engineering Aspects 198–200 (2002) 577–591.
[8] B. Liedberg, Z. Yang, I. Engquist, Journal of Physical Chemistry B 101 (1997) 5951–5962.
[9] H. Ahn, M. Kim, D.J. Sandman, J.E. Whitten, Langmuir 19 (2003) 5303–5310.
[10] A. Ulman, Chemical Reviews 96 (1996) 1533–1554.
[11] J.C. Love, L. a Estroff, J.K. Kriebel, R.G. Nuzzo, G.M. Whitesides, Chemical Reviews 105 (2005) 1103–1169.
[12] M. Magoga, C. Joachim, Physical Review B 56 (1997) 4722–4729.
[13] F. Biscarini, P. Samorı, O. Greco, R. Zamboni, Physical Review Letters 78 (1997) 2389–2392.
[14] A. Shehu, S. Quiroga, P. D'Angelo, C. Albonetti, F. Borgatti, M. Murgia, A. Scorzoni, P. Stoliar, F. Biscarini, Physical Review Letters 104 (2010) 1–4.
[15] Z.W. Lai, S. Das Sarma, Physical Review Letters 66 (1991) 2348–2351.
[16] S. Verlaak, S. Steudel, P. Heremans, D. Janssen, M.S. Deleuze, Physical Review B 68 (2003) 1–11.
[17] D. Käfer, L. Ruppel, G. Witte, Physical Review B 75 (2007) 085309 (1–14).
[18] Y. Shen, A.R. Hosseini, M.H. Wong, G.G. Malliaras, Chemphyschem: A European Journal of Chemical Physics and Physical Chemistry 5 (2004) 16–25.
[19] C. Bock, D.V. Pham, U. Kunze, D. Kafer, G. Witte, C. Woll, Journal of Applied Physics 100 (2006) 114517. 1-7.
[20] M.M. Thuo, W.F. Reus, C. a Nijhuis, J.R. Barber, C. Kim, M.D. Schulz, G.M. Whitesides, Journal of the American Chemical Society 133 (2011) 2962–2975.
[21] W. Porzio, S. Destri, M. Mascherpa, S. Bruckner, Acta Polymerica 44 (1993) 266–272.
[22] P. Ostoja, S. Guerri, S. Rossini, M. Servidori, C. Taliani, Synthetic Metals 54 (1993) 447–452.
[23] G. Wang, T.-W. Kim, Y.H. Jang, T. Lee, Journal of Physical Chemistry C 112 (2008) 13010–13016.
[24] W. Wang, T. Lee, M. aReed, The Journal of Physical Chemistry B 108 (2004) 18398–18407.
[25] J. Zaumseil, K.W. Baldwin, J.A. Rogers, Journal of Applied Physics 93 (2003) 6117–6124.
[26] P.V. Pesavento, R.J. Chesterfield, C.R. Newman, C.D. Frisbie, Journal of Applied Physics 96 (2004) 7312.
[27] K.P. Puntambekar, P.V. Pesavento, C.D. Frisbie, Applied Physics Letters 83 (2003) 5539.
[28] M. Walczak, D.D. Popenoe, R.S. Deinhammer, B.D. Lamp, C. Chung, M.D. Porter, Langmuir 7 (1991) 2687–2693.
[29] G. Zotti, S. Zecchin, B. Vercelli, A. Berlin, S. Grimoldi, L. Groenendaal, R. Bertoncello, M. Natali, Chemistry of Materials 17 (2005) 3681–3694.
[30] R. Michalitsch, A. Elkassmi, A. Yassar, F. Gamier, Journal of Heterocyclic Chemistry 38 (2001) 649–653.
[31] R.M. Kellogg, A.P. Schaap, E.T. Harper, H. Wynbert, The Journal of Organic Chemistry 33 (1968) 2902–2909.